

Supervised and Penalized Baseline Correction

Erik Andries^{*} ^{1,2} and Ramin Nikzad-Langerodi[†] ³

¹ *Center for Advanced Research Computing*
University of New Mexico, Albuquerque, NM, USA

² Central New Mexico Community College, Albuquerque, NM, USA

³ *Data Science Group*
Software Competence Center Hagenberg (SCCH) GmbH, Hagenberg, Austria

Abstract

Spectroscopic measurements can show distorted spectral shapes arising from a mixture of absorbing and scattering contributions. These distortions (or baselines) often manifest themselves as non-constant offsets or low-frequency oscillations. As a result, these baselines can adversely affect analytical and quantitative results. Baseline correction is an umbrella term where one applies pre-processing methods to obtain baseline spectra (the unwanted distortions) and then remove the distortions by differencing. However, current state-of-the-art baseline correction methods do not utilize analyte concentrations even if they are available, or even if they contribute significantly to the observed spectral variability. We examine a class of state-of-the-art methods (penalized baseline correction) and modify them such that they can accommodate a priori analyte concentrations such that prediction can be enhanced. Performance will be assessed on two near infra-red data sets across both classical penalized baseline correction methods (without analyte information) and modified penalized baseline correction methods (leveraging analyte information).

Keywords— Baseline correction, penalty terms, alternating least squares

^{*}Corresponding author: erik.andries@gmail.com

[†]ramin.nikzad-langerodi@scch.at

1 Introduction

Spectroscopic measurements, e.g., those obtained from near infrared (NIR) instrumentation, often show distorted spectral shapes arising from a mixture of absorbing and scattering contributions. NIR spectral scattering is caused by differences in path length due to physical artifacts where light ballistically deviates from a straight line into one or multiple paths with no absorption. Spectrally, this scattering typically manifests itself as undulating alterations, i.e., non-constant offsets and low frequency curves; see [1] for a catalogue of spectral distortions due to scattering. These scattering distortions can adversely affect qualitative or quantitative analytical results. The phrase *baseline correction* refers to pre-processing methods that remove the physical artifacts in spectra due to scattering. As a consequence of baseline removal, subsequent chemical interpretation and quantitative analyses is then more valid and applicable.

Historically, a common method for baseline correction is to fit a quadratic or higher-order polynomial function to each spectrum and then use the difference between the spectrum and the fitted function as the corrected spectrum [2–5]. For example, Multiplicative Scatter Correction (MSC) is one such procedure: it corrects each measured spectrum using fitted coefficients (slope and intercept) of a reference spectrum [6]. (The reference spectrum is usually just the average spectrum of the calibration set.) There are extensions to MSC (e.g., Extended MSC) that include first-order and/or second-order polynomial fitting to the reference spectrum and wavelength axis [7, 8].

Alternatively, baseline removal can also be achieved via derivative spectra (i.e., a scaled version of the first or second derivative of the original spectra). Differentiation removes low-frequency components (e.g., the second derivative removes constant and linear baselines). However, differentiation also introduces several problems. The numerical derivative can amplify noise and requires smoothing beforehand, with the final results being highly dependent on the parameters of the smoothing algorithm. Savitzky-Golay (SG) filtering, based on local least-squares fitting of the data by polynomials, is perhaps the most well-known method in chemometrics for smoothing and computing derivatives on noisy data [9]. Although SG is a common technique for baseline removal, SG filtering can unnecessarily reduce the signal-to-noise ratio, and is prone to artifacts at the end of the wavelength range [10]. Hence, derivative-based baseline removal often amounts to a balancing act—it must be smooth enough to “clean up” unwanted noise, but not so much as to remove important spectral gradients.

Our particular interest is in the class of derivative smoothers that has its roots in the penalized least squares approach of Eilers [11]. Later penalized variants extended the Eilers approach by using weighted least squares generalizations that iteratively updated the baseline for a given spectrum [12–14]. However, what is peculiar about these state-of-the-art penalized baseline correction methods is the following observation: they do not consider analyte concentrations across samples. This is curious because strongly absorbing or scattering analytes, possibly distinct from the

response variable or analyte of interest, can dominate or strongly influence the observed spectral variability.¹ For example, biological samples contain considerable moisture content, and water absorbance often dominates the observed spectral variability across multiple bands in the NIR spectra. However, this moisture information is not considered for baseline correction purposes even when reference measurements for moisture are available. In short, current baseline correction methods are unsupervised in that they are agnostic with respect to analyte concentrations.

We propose how current penalized baseline correction methods can be modified to accommodate reference measurements associated with strongly absorbing or strongly scattering analytes. We call our proposed approach *Supervised Penalized Baseline Correction* (SPBC). In Section 2, we discuss current methods of penalized baseline correction. In Section 3, we propose a modification that can accommodate reference measurements. Section 4 describes the data sets and the performance metrics used for assessment, and details the procedure for selecting tuning parameters. Section 5 evaluates performance on a suite of baseline correction tasks using two NIR data sets. Section 6 states the the conclusion and suggestions for future work.

Notation. In this paper, matrices and vectors are denoted by uppercase and lowercase letters in boldface (e.g., \mathbf{X} and \mathbf{x}). The superscripts T and $^+$ indicate the transpose and pseudoinverse, respectively, and the superscript $^{-1}$ indicates the inverse of a matrix. The column and row of a matrix are denoted by the following subscripts: $\mathbf{x}_{i\cdot}$ is the i th row of \mathbf{X} , while $\mathbf{x}_{\cdot j}$ is the j th column of \mathbf{X} . All vectors are column vectors unless indicated otherwise. The comma and semicolon will be used to indicate horizontal and vertical concatenation. For example, an $m \times n$ matrix of spectra \mathbf{X} can be written as m samples aligned horizontally ($\mathbf{X} = [\mathbf{x}_{1\cdot}; \dots; \mathbf{x}_{m\cdot}]$) or as m samples aligned vertically and then transposed ($\mathbf{X} = [\mathbf{x}_{\cdot 1}, \dots, \mathbf{x}_{\cdot m}]^T$). Here, each sample is n -dimensional: $\mathbf{x}_{\cdot i} = [x_{1i}; \dots; x_{ni}]$ or $\mathbf{x}_{i\cdot} = [x_{1i}, \dots, x_{ni}]^T$. The vector $\mathbf{y} = [y_1; \dots; y_m]$ or $\mathbf{y} = [y_1, \dots, y_m]^T$ corresponds to an $m \times 1$ vector of reference measurements such that y_i corresponds to $\mathbf{x}_{i\cdot}$. We will also denote another analyte $\mathbf{a} = [a_1; \dots; a_m]$ or $\mathbf{a} = [a_1, \dots, a_m]^T$ distinct from \mathbf{y} to indicate a strongly absorbing or scattering analyte.

2 Penalized Baseline Correction

The approach discussed here relies on penalized least squares (or Tikhonov regularization in mathematical parlance) and borrows heavily from the algorithmic machinery in [11]. We will use the phrase *Penalized Baseline Correction* (PBC) to collectively refer to the spectroscopic baseline correction approaches discussed by Paul Eilers in [11] and later variants discussed in Section 2.2.

¹An earlier paper [3] did consider analyte concentrations via a different class of smoothing, but its regime of applicability was quite restrictive: a mixture of solvents in which the concentrations of all component species—other than the analyte of interest—is known.

2.1 Single Spectrum Formulation of Eilers

Suppose \mathbf{x} indicates a spectrum from a sample and \mathbf{z} denotes the baseline correction vector to be fitted or solved for. The misfit between \mathbf{x} and \mathbf{z} can be expressed as $\|\mathbf{x} - \mathbf{z}\|_2^2$. However, we want \mathbf{z} to be smooth, and as a result, the roughness can be controlled by introducing a penalty term such that we seek to minimize the following function [11]

$$f(\mathbf{z}) = \|\mathbf{x} - \mathbf{z}\|_2^2 + \lambda^2 \|\mathbf{D}\mathbf{z}\|_2^2 = (\mathbf{x} - \mathbf{z})^T(\mathbf{x} - \mathbf{z}) + \lambda^2 \mathbf{z}^T \mathbf{C} \mathbf{z}, \quad \mathbf{C} = \mathbf{D}^T \mathbf{D}, \quad \lambda > 0, \quad (1)$$

where the matrix \mathbf{D} is termed the discrete smoothing operator [15]. The matrix \mathbf{D} typically takes on one of two forms— \mathbf{D}_1 or \mathbf{D}_2 —where the matrices

$$\mathbf{D}_1 = \begin{bmatrix} 1 & -1 & & \\ & \ddots & \ddots & \\ & & 1 & -1 \end{bmatrix} \in \mathbb{R}^{(n-1) \times n} \quad \text{and} \quad \mathbf{D}_2 = \begin{bmatrix} 1 & -2 & 1 & \\ & \ddots & \ddots & \ddots \\ & & 1 & -2 & 1 \end{bmatrix} \in \mathbb{R}^{(n-2) \times n} \quad (2)$$

are scaled approximations to the first and second derivative operators. In the case of the first derivative operator where $\mathbf{D} = \mathbf{D}_1$, one can express the two-norm penalty in Eq.(1) as $\|\mathbf{D}_1 \mathbf{z}\|_2^2 = \sum_{i=1}^{n-1} (z_i - z_{i+1})^2$. By setting the gradient of $f(\mathbf{z})$ in Eq.(1) equal to $\mathbf{0}$, we arrive at the linear system:

$$\nabla f(\mathbf{z}) = \mathbf{0} \quad \Rightarrow \quad (\mathbf{I} + \lambda^2 \mathbf{C}) \mathbf{z} = \mathbf{x}. \quad (3)$$

When $\lambda = 0$, then $\mathbf{z} = \mathbf{x}$; but this would be a non-sensical choice since the baseline-corrected spectra would be $\mathbf{x} - \mathbf{z} = \mathbf{0}$. Hence, small values of λ (i.e., $\lambda \ll 1$) are not recommended.

2.2 Weighted Variants

To introduce flexibility, one can weight the misfit term $\|\mathbf{x} - \mathbf{z}\|_2^2$ in Eq.(1) with a diagonal matrix $\mathbf{H} = \text{diag}(h_1, h_2, \dots, h_n)$ containing non-negative weight entries:

$$g(\mathbf{z}) = \|\mathbf{H}^{1/2}(\mathbf{x} - \mathbf{z})\|_2^2 + \lambda^2 \|\mathbf{D}\mathbf{z}\|_2^2 = (\mathbf{x} - \mathbf{z})^T \mathbf{H}(\mathbf{x} - \mathbf{z}) + \lambda^2 \mathbf{z}^T \mathbf{C} \mathbf{z} \quad (4)$$

$$\nabla g(\mathbf{z}) = \mathbf{0} \quad \Rightarrow \quad (\mathbf{H} + \lambda^2 \mathbf{C}) \mathbf{z} = \mathbf{H} \mathbf{x}.$$

Subsequent PBC variants of [12–14] (known as ASLS, AIRPLS and ARPLS, respectively) go much further and construct a separate weight matrix for each sample $\mathbf{x}_{:i}$. Moreover, each sample-specific weight matrix is also iteratively updated such that the normal equations in Eq.(4) become

$$(\mathbf{H}_i^k + \lambda^2 \mathbf{C}) \mathbf{z}_{:i}^k = \mathbf{H}_i^k \mathbf{x}_{:i}.$$

where i and k correspond to the i^{th} sample and k^{th} iteration, respectively. Likewise, the baseline vector $\mathbf{z}_{:i}^k = [z_1^k, z_2^k, \dots, z_n^k]^T$ denotes the baseline-corrected spectrum constructed for the i^{th} sample $\mathbf{x}_{:i} = [x_1, x_2, \dots, x_n]^T$ at the k^{th} iteration. The $n \times n$ diagonal weight matrix is expressed as $\mathbf{H}_i^k =$

$\text{diag}(h_{i1}^k, h_{i2}^k, \dots, h_{in}^k)$. For example, AIRPLS updates the j^{th} diagonal weight (associated with the j^{th} wavelength) in the following fashion:

$$h_{ij}^k = \begin{cases} 0, & x_j \geq z_j^{k-1} \\ \exp(k(x_j - z_j^{k-1})/\rho), & x_j < z_j^{k-1} \end{cases} \quad \text{where} \quad \rho = \sum_{l=1}^n \min(0, x_l - z_l^{k-1}).$$

ASLS and ARPLS use different mechanisms to update the diagonal weight entries in \mathbf{H}_i^k .

Figure 1 illustrates the sequence of baseline correction using AIRPLS: the original spectra, the baselines, and the baseline-corrected spectra on the cookie data set (see Section 4.1.1 for a description of this data set). The left-most subplot displays the spectra where the colored lines indicate the level of water concentration—as displayed in the colorbar to the immediate right. (With respect to baseline correction, water is the analyte of interest to be discussed later in this paper.) The middle two subplots display the baseline spectra constructed from \mathbf{D}_1 and \mathbf{D}_2 , and the right-most two subplots display the baseline-corrected spectra for \mathbf{D}_1 and \mathbf{D}_2 . This figure highlights the basic question: for regression purposes, is it better to use the original spectra \mathbf{X} or the baseline-corrected spectra ($\mathbf{X} - \mathbf{Z}_1$ or $\mathbf{X} - \mathbf{Z}_2$)? The key observation is the following for the variant PBC approaches: whereas the Eilers approach applies the same baseline correction procedure to each of the m spectra $\mathbf{x}_{:,i}$ (via pre-multiplication by $(\mathbf{I} + \lambda^2 \mathbf{C})^{-1}$), the weighted PBC variants perform m different but simultaneous baseline corrections in parallel.

2.3 Multiple Spectrum Formulation

Instead of operating on one spectrum at a time, we extend Eq.(1) and Eq.(4) to accommodate an entire $m \times n$ matrix of spectra \mathbf{X} and an entire $m \times n$ matrix of baselines \mathbf{Z} where $\mathbf{z}_{i,:}$ is the baseline associated with $\mathbf{x}_{i,:}$. This can be accomplished using the Frobenius norm:

$$f(\mathbf{Z}) = \|\mathbf{X} - \mathbf{Z}\|_F^2 + \lambda^2 \|\mathbf{DZ}^T\|_F^2. \quad (5)$$

The Frobenius norm of an $m \times n$ matrix \mathbf{A} is expressed as $\|\mathbf{A}\|_F^2 = \sum_{i=1}^m \sum_{j=1}^n a_{ij}^2$ and can be thought of as a two-norm on the “flattened version” of \mathbf{A} where the flattened vector \mathbf{A} now has

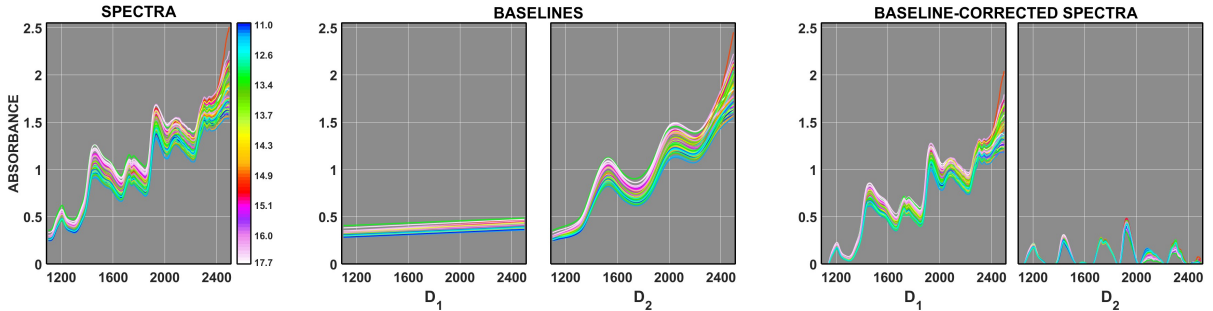


Figure 1: For the cookie data set, we display the spectra (left subplot), AIRPLS baselines with $\lambda = 100$ via \mathbf{D}_1 and \mathbf{D}_2 (middle subplots), and the corresponding baseline-corrected spectra (right subplots).

size $mn \times 1$. Setting the gradient of Eq.(5) equal to zero (in addition to its weighted equivalent in Eq.(4)), we obtain the subsequent normal equations [16]:

$$\begin{aligned}\nabla f(\mathbf{Z}) = \mathbf{0} &\Rightarrow \mathbf{Z}(\mathbf{I} + \lambda^2 \mathbf{C}) = \mathbf{X}, \\ \nabla g(\mathbf{Z}) = \mathbf{0} &\Rightarrow \mathbf{Z}(\mathbf{H} + \lambda^2 \mathbf{C}) = \mathbf{X}\mathbf{H}.\end{aligned}\tag{6}$$

The equations in Eq.(6) are essentially the same as in Eqs.(3,4) but the coefficient matrices $\mathbf{I} + \lambda^2 \mathbf{C}$ and $\mathbf{H} + \lambda^2 \mathbf{C}$ are applied to all baseline spectra simultaneously as opposed to one spectrum at a time. Note that in Eqs.(3,4), the spectra \mathbf{x} and \mathbf{z} are column vectors while the collective spectra in \mathbf{X} and \mathbf{Z} are aligned row-wise. To maintain alignment consistency with Eqs.(3,4), one could rewrite the equations in a column-wise format, e.g., $(\mathbf{I} + \lambda^2 \mathbf{C})\mathbf{Z}^T = \mathbf{X}^T$ and $(\mathbf{H} + \lambda^2 \mathbf{C})\mathbf{Z}^T = \mathbf{H}\mathbf{X}^T$.

3 Supervised Penalized Baseline Correction

In Sections 2.1 and 2.3, only the matrix \mathbf{X} is used to construct the baseline matrix \mathbf{Z} . However, the approach in Section 2.3 can be modified to accommodate a priori analyte information. The forthcoming *supervised PBC* approaches will be denoted by the acronym SPBC. The first SPBC approach is based on Nonlinear Iterative Partial Least Squares (NIPALS) and will be denoted as SPBCN. The second approach is based on Inverse Least Squares (ILS) and will be denoted as SPBCI.

3.1 NIPALS framework of SPBCN

Let the vector $\mathbf{a} = [a_1, a_2, \dots, a_m]^T$ denote an analyte that will be used to construct the baseline. Here, we extend the Eilers approach via the NIPALS outer-product approach

$$\begin{aligned}f(\mathbf{w}, \mathbf{Z}) &= \|(\mathbf{X} - \mathbf{Z}) - \mathbf{a}\mathbf{w}^T\|_F^2 + \lambda^2 \|\mathbf{D}\mathbf{Z}^T\|_F^2 \\ &= \|\mathbf{R} - \mathbf{Z}\|_F^2 + \lambda^2 \|\mathbf{D}\mathbf{Z}^T\|_F^2, \quad \mathbf{R} = \mathbf{X} - \mathbf{a}\mathbf{w}^T.\end{aligned}\tag{7}$$

Note that the Eilers approach of Eq.(5) and the NIPALS extension in Eq.(7) are functionally equivalent with \mathbf{X} being swapped out for with \mathbf{R} in Eq.(7). In effect, SPBCN baseline-corrects the *residual* or deflated matrix \mathbf{R} instead of \mathbf{X} . (When $\mathbf{a} = \mathbf{0}$, SPBCN reduces to the Eilers approach.) Since Eq.(7) is now a function of two variables \mathbf{Z} , we set the gradients of $f(\mathbf{w}, \mathbf{Z})$ —separately with respect to \mathbf{w} and \mathbf{Z} —equal to zero and obtain:

$$\begin{aligned}\nabla_{\mathbf{w}} f = 0 &\Rightarrow \mathbf{w} = \frac{(\mathbf{X} - \mathbf{Z})^T \mathbf{a}}{\mathbf{a}^T \mathbf{a}} \\ \nabla_{\mathbf{Z}} f = 0 &\Rightarrow \mathbf{Z} = \mathbf{R}(\mathbf{I} + \lambda^2 \mathbf{C})^{-1}.\end{aligned}\tag{8}$$

The above equations can now be solved via alternating least squares (ALS): solve for \mathbf{w} in the $\nabla_{\mathbf{w}} f = 0$ step, plug in the resultant \mathbf{w} in the equations associated with $\nabla_{\mathbf{Z}} f = 0$ and solve for \mathbf{Z} . The pseudocode for this ALS approach is given in Algorithm 1. The most computationally intensive

step in the pseudocode occurs in Step 4, i.e., solve $\mathbf{Z}_{(k+1)} = \mathbf{R}(\mathbf{I} + \lambda^2 \mathbf{C})^{-1}$. In the classical PBC approach of Eilers in Eq.(1), sparse matrix linear libraries coupled with Cholesky factorization was used to efficiently solve the linear system. However, a much faster numerical implementation can be performed, particularly in the case of $\mathbf{D} = \mathbf{D}_1$; see Section C of the Supplement.

Algorithm 1 SPBCN

input: \mathbf{X} , \mathbf{a} , λ , $\mathbf{C} = \mathbf{D}^T \mathbf{D}$
initialize: $k = 0$, $\mathbf{Z}_{(k)} = \mathbf{0}$
while not converged **do**
 Step 1: $\mathbf{B} = \mathbf{X} - \mathbf{Z}_{(k)}$
 Step 2: $\mathbf{w} = \frac{\mathbf{B}^T \mathbf{a}}{\mathbf{a}^T \mathbf{a}}$
 Step 3: $\mathbf{R} = \mathbf{X} - \mathbf{a} \mathbf{w}^T$
 Step 4: $\mathbf{Z}_{(k+1)} = \mathbf{R}(\mathbf{I} + \lambda^2 \mathbf{C})^{-1}$
 Step 5: $k = k + 1$
end while
return $\mathbf{Z} = \mathbf{Z}_{(k+1)}$

Figure 2 gives an example of the SPBCN-based baseline correction process for the cookie data set where water concentrations in \mathbf{a} are used to construct the baselines. Compared to Figure 1 where baseline correction via AIRPLS was performed, the baseline-corrected spectra via SPBC exhibit a more sequential arrangement of spectra as a function of water concentration—as absorbance increases for a particular wavelength, the spectral values increase in concentration.

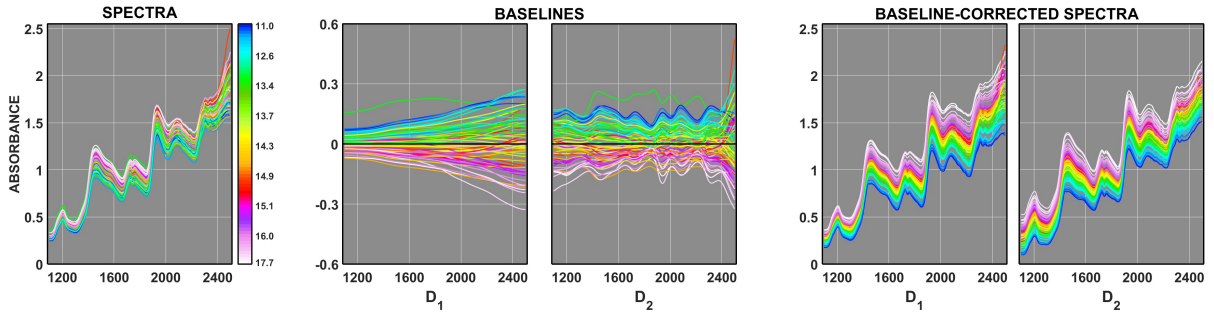


Figure 2: Spectra, baseline spectra and baseline-corrected spectra for the first and second derivative operators (\mathbf{D}_1 and \mathbf{D}_2) when using SPBCN.

3.2 ILS framework of SPBCI

Instead of the outer product approach of SPBCN, we can employ an inner product approach via ILS to extend Eq.(5):

$$\begin{aligned} f(\mathbf{w}, \mathbf{Z}) &= \|(\mathbf{X} - \mathbf{Z})\mathbf{w} - \mathbf{a}\|_2^2 + \lambda^2 \|\mathbf{DZ}^T\|_F^2 \\ &= \|\mathbf{Z}\mathbf{w} - \mathbf{r}\|_2^2 + \lambda^2 \|\mathbf{DZ}^T\|_F^2, \quad \mathbf{r} = \mathbf{X}\mathbf{w} - \mathbf{a}. \end{aligned} \quad (9)$$

Here, we are trying to relate the baseline corrected spectra $\mathbf{X} - \mathbf{Z}$ to the analyte concentrations in \mathbf{a} via the regression vector $\mathbf{w} = [w_1, w_2, \dots, w_n]^T$. As with Eq.(7), we set of the gradients, separately with respect to \mathbf{w} and \mathbf{Z} , equal to zero and obtain:

$$\begin{aligned} \nabla_{\mathbf{w}} f &= 0 \quad \Rightarrow \quad \mathbf{w} = [(\mathbf{X} - \mathbf{Z})^T(\mathbf{X} - \mathbf{Z})]^+ (\mathbf{X} - \mathbf{Z})^T \mathbf{a} \\ \nabla_{\mathbf{Z}} f &= 0 \quad \Rightarrow \quad \mathbf{Z} = \mathbf{r}\mathbf{w}^T (\mathbf{w}\mathbf{w}^T + \lambda^2 \mathbf{C})^{-1}. \end{aligned} \quad (10)$$

The pseudocode for SPBCI via ALS is given in Algorithm 2. The most computationally intensive steps in the pseudocode occurs in Steps 2 and 4, i.e., solve $\mathbf{B}^T \mathbf{B} \mathbf{w} = \mathbf{B}^T \mathbf{a}$ for \mathbf{w} and $\mathbf{Z}_{(k+1)} = \mathbf{r}\mathbf{w}^T (\mathbf{w}\mathbf{w}^T + \lambda^2 \mathbf{C})^{-1}$, respectively. See Section C in the Supplement for details on how these steps were numerically implemented.

Algorithm 2 SPBCI

input: $\mathbf{X}, \mathbf{a}, \lambda, \mathbf{C} = \mathbf{D}^T \mathbf{D}$
initialize: $k = 0, \mathbf{Z}_{(k)} = \mathbf{0}, \mathbf{w}_{(k)} = \mathbf{0}$
while not converged **do**
 Step 1: $\mathbf{B} = \mathbf{X} - \mathbf{Z}_{(k)}$
 Step 2: Solve $\mathbf{B}^T \mathbf{B} \mathbf{w} = \mathbf{B}^T \mathbf{a}$ for \mathbf{w}
 Step 3: $\mathbf{r} = \mathbf{X}\mathbf{w} - \mathbf{a}$
 Step 4: $\mathbf{Z}_{(k+1)} = \mathbf{r}\mathbf{w}^T (\mathbf{w}\mathbf{w}^T + \lambda^2 \mathbf{C})^{-1}$
 Step 5: $k = k + 1$
end while
return $\mathbf{Z} = \mathbf{Z}_{(k+1)}$

3.3 Sample Dependence

In the Eilers approach where $\mathbf{z}_{:i} = (\mathbf{I} + \lambda^2 \mathbf{C})^{-1} \mathbf{x}_{:i}^T$, the baseline correction procedure for each spectrum $\mathbf{x}_{:i}^T$ is the same, i.e., pre-multiplication by $(\mathbf{I} + \lambda^2 \mathbf{C})^{-1}$. In the weighted variants (e.g., ASLS AIRPLS or ARPLS), $\mathbf{z}_{:i} = (\mathbf{H}_i^k + \lambda^2 \mathbf{C})^{-1} \mathbf{H}_i^k \mathbf{x}_{:i}^T$, and as a result, the baseline correction procedure is the not the same for each spectrum. However, like the Eilers approach, baseline correction for any one spectrum $\mathbf{x}_{:i}$ can be done in parallel, (i.e., the baseline correction done

one spectrum does not depend on the baseline correction done on another spectrum). Baseline correction for SPBC approaches, on the other hand, cannot be done one spectrum at a time. They must be done in batch fashion. Thus, the baseline for each sample encodes information (on analyte concentration) across the entire calibration set which is in contrast to previous approaches.

4 Experimental Methods

4.1 Data Sets

We will examine two near infrared (NIR) data sets: the milk and cookie data sets. The NIR spectra for these data sets are displayed in Figure 3.

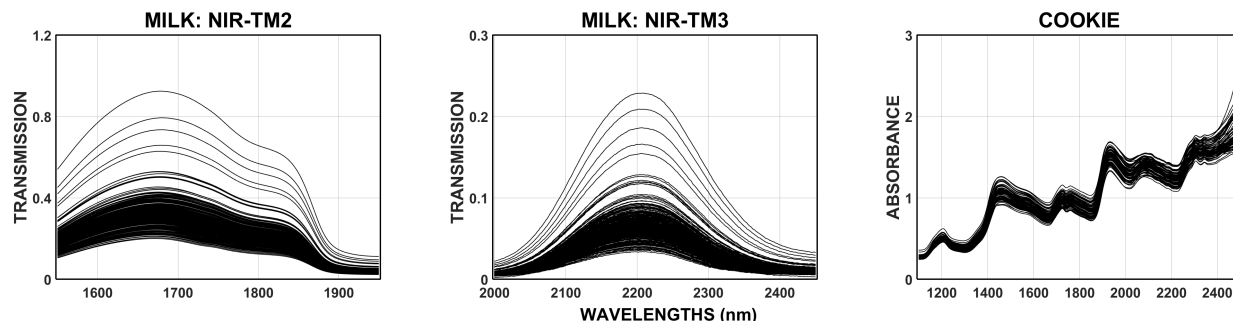


Figure 3: Spectra for the milk data set (instruments NIR-TM2 and NIR-TM3 in transmission mode) and the cookie data set (in absorbance mode) on the far right.

4.1.1 Cookie Data Set

The cookie data set contains measurements from quantitative NIR spectroscopy [17]. The intent of using this data set is to test the feasibility of NIR spectroscopy to measure the composition of biscuit dough pieces. There are four analytes under consideration: fat, sucrose, flour, and water. The calculated percentages of these four ingredients represent the four response variables. There are 72 samples in total: 40 samples in the calibration set (with sample 23 being an outlier) and 32 samples in the separate prediction or validation set (with example 21 considered as an outlier). An NIR reflectance spectrum is available for each dough piece. The spectral data consist of 700 points measured from 1100 to 2498 nanometers (nm) in intervals of 2nm. In this data set, sucrose will be the response variable (y) to be predicted, while fat, water and flour will each separately be the analyte a that will be used to construct the baselines.

4.1.2 Milk Data Set

The milk data set consists of 298 samples measured across three separate Microelectromechanical System (MEMS) NIR spectrometers in transmission mode [18]. The three spectrometers are denoted in this paper as NIR-TM1, NIR-TM2 and NIR-TM3. The spectrum for each milk sample is an average of 20 replicates. NIR-TM1, NIR-TM2 and NIR-TM3 span 1100-1400nm, 1550-1950nm and 2000-2450nm, respectively, with an interval of 2nm. There are six primary analytes under consideration: fat, lactose, protein, urea, solute and dry matter. We will focus on instruments NIR-TM2 and NIR-TM3. In this data set, fat will be the analyte (\mathbf{a}) that will be used to construct the baselines. Lactose, protein, urea, solute and dry matter will each separately be the response variable or analyte \mathbf{y} to be predicted.

4.2 Schemes involving the availability of \mathbf{a}

The SPBC implementation depends on how much information associated with the analyte \mathbf{a} is available. Data-wise, we will use the triplet $\{\mathbf{X}, \mathbf{a}, \mathbf{y}\}$. The $m \times n$ matrix \mathbf{X} denotes the spectra to be baseline corrected, the $m \times 1$ vector \mathbf{a} corresponds to the analyte that will be used for baseline correction, and the $m \times 1$ vector \mathbf{y} corresponds to the response variable or analyte whose concentrations we want to predict. We will split the data into three parts: the calibration (or training), tuning, and validation (or test) sets, which will be denoted by the subscripts 1, t and 2, i.e., $\{\mathbf{X}_1, \mathbf{a}_1, \mathbf{y}_1\}$, $\{\mathbf{X}_t, \mathbf{a}_t, \mathbf{y}_t\}$ and $\{\mathbf{X}_2, \mathbf{a}_2, \mathbf{y}_2\}$. The tuning set will be aside and will be exclusively used to estimate the number of PLS latent dimensions. See Section 4.4 for a more detailed explanation of how the data is partitioned. Ultimately, our goal is to enhance the prediction of \mathbf{y}_2 by utilizing baseline corrected spectra constructed from $\mathbf{X} := [\mathbf{X}_1; \mathbf{X}_2]$ and $\mathbf{a} := [\mathbf{a}_1; \mathbf{a}_2]$. (The symbol “:=” typically denotes that the left-hand side is defined as the expression on the right-hand side.) The prediction of \mathbf{y}_2 proceeds in two steps to be described next.

4.2.1 Full and Partial Schemes

We use $\mathbf{X} := [\mathbf{X}_1; \mathbf{X}_2]$ and $\mathbf{a} := [\mathbf{a}_1; \mathbf{a}_2]$ in algorithms 1 or 2 to obtain \mathbf{Z} , and then split it into two parts \mathbf{Z}_1 and \mathbf{Z}_2 corresponding to the calibration and validation sets such that $\mathbf{Z} := [\mathbf{Z}_1; \mathbf{Z}_2]$. Computing \mathbf{Z}_1 and \mathbf{Z}_2 requires \mathbf{a}_1 and \mathbf{a}_2 , respectively. The *full scheme* assumes that we have full access to both $[\mathbf{X}_1; \mathbf{X}_2]$ and $[\mathbf{a}_1; \mathbf{a}_2]$. (Suppose the reference measurements for both \mathbf{a}_1 and \mathbf{a}_2 are inexpensive and/or easy to obtain with respect to laboratory effort and time, then $\mathbf{X} := [\mathbf{X}_1; \mathbf{X}_2]$ and $\mathbf{a} := [\mathbf{a}_1; \mathbf{a}_2]$ will be the inputs into Algorithms 1 and 2). The *partial scheme* assumes that we have full access to $\mathbf{X} := [\mathbf{X}_1; \mathbf{X}_2]$ but only partial access to \mathbf{a} , that is we have knowledge of \mathbf{a}_1 but not \mathbf{a}_2 . Without access to \mathbf{a}_2 , however, we will need reliable approximations or estimates to act as numerical proxies. Instead of using $\mathbf{a} := [\mathbf{a}_1; \mathbf{a}_2]$, we can use a combined set of known references \mathbf{a}_1 and prediction estimates $\hat{\mathbf{a}}_2$ such that $\hat{\mathbf{a}} := [\mathbf{a}_1; \hat{\mathbf{a}}_2]$. In short, for the partial scheme,

we use $\hat{\mathbf{a}}$ to construct the baselines instead of \mathbf{a} . Compared to the partial scheme, we can expect the construction of the baseline spectra for the full scheme to be qualitatively better since known references are used. Hence, the performance of the partial scheme will be highly dependent on the accuracy and precision associated with the estimates in $\hat{\mathbf{a}}_2$.

The construction of the estimates in $\hat{\mathbf{a}}_2$ proceeds as follows for each data partition. 80% of the samples are randomly sampled from the calibration set $\{\mathbf{X}_1, \mathbf{a}_1\}$. The calibration model is then applied to \mathbf{X}_2 and a prediction estimate $\hat{a}_2^{(1)}$ is obtained. Another 80% of the samples are randomly sampled from the calibration set, the subsequent model is then applied to \mathbf{X}_2 and another prediction estimate $\hat{a}_2^{(2)}$ is obtained. This process is repeated for a total of 25 times such that we obtain the following collection of estimates $\{\hat{a}_2^{(1)}, \hat{a}_2^{(2)}, \dots, \hat{a}_2^{(25)}\}$. The prediction estimates outside the “Tukey interval” (or $[Q_1 - 1.5(Q_3 - Q_1), Q_3 + 1.5(Q_3 - Q_1)]$) are removed and the remaining estimates are averaged to yield the final estimate for $\hat{\mathbf{a}}_2$.

4.2.2 Build calibration model and predict y_2

Once $\mathbf{Z} = [\mathbf{Z}_1; \mathbf{Z}_2]$ has been obtained, we baseline-correct the calibration and validation sets whereby $\mathbf{X}_1^{\text{BC}} = \mathbf{X}_1 - \mathbf{Z}_1$ and $\mathbf{X}_2^{\text{BC}} = \mathbf{X}_2 - \mathbf{Z}_2$, respectively. We mean-center the calibration set

$$\begin{aligned}\mu_x &= (\mathbf{1}_{n_1}^T \mathbf{X}_1^{\text{BC}}) / n_1, \quad \mathbf{X}_1^{\text{BC}} := \mathbf{X}_1^{\text{BC}} - \mathbf{1}_{n_1} \mu_x \\ \mu_y &= (\mathbf{1}_{n_1}^T \mathbf{y}_1) / n_1, \quad \mathbf{y}_1 := \mathbf{y}_1 - \mathbf{1}_{n_1} \mu_y,\end{aligned}$$

and solve $\mathbf{X}_1^{\text{BC}} \mathbf{b} = \mathbf{y}_1$ for \mathbf{b} using, for example, Partial Least Squares (PLS) regression. Finally, we then predict y_2 via

$$\hat{\mathbf{y}}_2 = (\mathbf{X}_2^{\text{BC}} - \mathbf{1}_{n_2} \mu_x) \mathbf{b} + \mathbf{1}_{n_2} \mu_y.$$

4.3 Baseline Correction Methods Examined

We will examine several classes of penalized smoothing methods: 1) no background correction (just using the original spectra without pre-processing); 2) the original PBC approach of Eilers in Section 2.1; 3) a PBC smoothing variant of Section 2.2; and 3) the SPBC methods introduced in Section 3. We outline them below:

- **NONE:** Here, no background correction is applied. However, from a background correction point of view, $\mathbf{Z} = \mathbf{0}$ and the baseline corrected spectra is simply $\mathbf{X} - \mathbf{Z} = \mathbf{X}$. **NONE** then serves as the benchmark by which the other baseline correction methods are intended to outperform.
- **EILERS:** This refers to the construction of the baseline spectra \mathbf{Z} by the original PBC approach of Eilers in Section 2.1.
- **AIRPLS:** The baseline spectra \mathbf{Z} are constructed via Adaptive Iteratively Reweighted Penalized Least Squares [13]. With respect to the other PBC variants mentioned in Section 2.2

(ASLS and ARPLS) that use weighted least squares, we observed that these variants performed qualitatively the same as AIRPLS. As a result, and for ease of illustration, we use AIRPLS as the canonical PBC variant.

- SPBC: The SPBC methods construct the baseline spectra \mathbf{Z} by accommodating analyte information. The SPBC approaches can be subdivided by approach (inverse least squares versus NIPALS) and by scheme (full versus partial):
 - SPBCI:F: Inverse least squares coupled with the full scheme.
 - SPBCI:P: Inverse least squares coupled with the partial scheme.
 - SPBCN:F: NIPALS coupled with the full scheme.
 - SPBCN:P: NIPALS coupled with the partial scheme.

We also explored the smoothing approaches of Savitsky-Golay (SG) and Extended Multiplicative Scatter Correction (EMSC) [6, 7, 9]. Here, our version of EMSC utilizes a “plain vanilla” approach that accounts for wavelength dependencies where the fitting coefficients β were modeled as

$$\mathbf{X}\beta = [\mathbf{1}, \mathbf{r}, \boldsymbol{\lambda}, \boldsymbol{\lambda}^2].$$

Here, \mathbf{r} is the reference spectrum and $\boldsymbol{\lambda} = [\lambda_1, \lambda_2, \dots, \lambda_n]^T$ is the vector of wavelengths. Although we have knowledge of the concentrations of many analytes, we do not assume that we have enough knowledge across the major chemical constituents (analytes and interferents) in the milk and cookie data sets; hence the rationale for employing the basic EMSC approach accounting only for wavelength dependencies. We found that SG and EMSC were inferior to AIRPLS in all instances (and in the case of SG, we even tried to optimize for frame length, or moving window width). As a consequence, and as was the case with ASLS and ARPLS, we also do not display performance results for SG and EMSC.

4.4 Data Partitions and Assessment Metrics

To ensure that performance results are not anecdotal to one particular split of the data, we assess the performance across 200 splits of the data. Each partition of the m samples randomly shuffles the data and splits it into three sets: 45% (calibration), 5% (tuning) and 50% (validation or testing). The first 45% of the samples will be used to build the calibration model. The next 5% of the samples belong to the tuning set. The prediction of \mathbf{y} on the tuning set samples will be used to select the PLS latent dimension that will subsequently be applied to the validation set. Aside from the tuning set, we split the samples into two sets of triplets: the calibration triplet $\{\mathbf{X}_1, \mathbf{y}_1, \mathbf{a}_1\}$ —derived from the 45% block of samples—and the validation triplet $\{\mathbf{X}_2, \mathbf{y}_2, \mathbf{a}_2\}$ —derived from the 50% block of samples. Note that the SPBC partial scheme uses the validation triplet $\{\mathbf{X}_2, \mathbf{y}_2, \hat{\mathbf{a}}_2\}$ where $\hat{\mathbf{a}}_2$ is a proxy or prediction estimate for \mathbf{a}_2 .

To assess the performance for the i^{th} partition or data split, we use two metrics: MARD and the coefficient of determination (R^2). MARD is an acronym for Mean Absolute Relative Difference, and is computed as the mean value of the absolute relative difference (ARD) between prediction estimates and reference measurements. For example, MARD for the validation set would be computed as follows: the predictions and reference measurements for the i^{th} partition are defined as $\hat{\mathbf{y}}_2 = [\hat{y}_{2,1}^{(i)}, \dots, \hat{y}_{2,m_2}^{(i)}]^T$ and $\mathbf{y}_2 = [y_{2,1}^{(i)}, \dots, y_{2,m_2}^{(i)}]^T$, respectively, and

$$\text{ARD}_j^{(i)} = 100\% \left| \frac{\hat{y}_{2,j}^{(i)} - y_{2,j}^{(i)}}{y_{2,j}^{(i)}} \right|, \quad \text{MARD}^{(i)} = \frac{1}{m_2} \sum_{j=1}^{m_2} \text{ARD}_j^{(i)}.$$

To compute MARD for the tuning set, one would instead replace $\hat{\mathbf{y}}_2$ and \mathbf{y}_2 with $\hat{\mathbf{y}}_t = [\hat{y}_{t,1}^{(i)}, \dots, \hat{y}_{t,m_t}^{(i)}]^T$ and $\mathbf{y}_t = [y_{t,1}^{(i)}, \dots, y_{t,m_t}^{(i)}]^T$, respectively. MARD basically functions as an aggregate percent relative error measure across a set of samples. The coefficient of determination metric derives from the line-of-best-fit in the scatter diagram associated with the coordinates

$$\{ (y_{2,1}^{(i)}, \hat{y}_{2,1}^{(i)}), (y_{2,2}^{(i)}, \hat{y}_{2,2}^{(i)}), \dots, (y_{2,m_2}^{(i)}, \hat{y}_{2,m_2}^{(i)}) \}$$

between the reference measurements and prediction estimates. The coefficient of determination for the i^{th} partition will be denoted as $R2^{(i)}$. We then create boxplots from the collection of $\text{MARD}^{(i)}$ and $R2^{(i)}$ measures across the partitions $i \in \{1, 2, \dots, 200\}$. Instead of the traditional boxplots where the inter-quartile range is the middle 50% of the data, we modify our boxplots to show the middle 80% where the edges of the “box” correspond to the 10% and 90% percentiles. Moreover, no outliers are displayed; instead the whiskers extend to the min and max of the data.

4.5 Selection of λ values

In the penalized methods associated with Eilers, the PBC variants such as AIRPLS, and the SPBC approaches, the value of λ is the tuning parameter of interest. The simplicity of the Eilers approach, i.e., $\mathbf{Z}(\mathbf{I} + \lambda^2 \mathbf{C}) = \mathbf{X}$, yields insight on what a reasonable choice λ should be. When λ is small ($0 < \lambda \ll 1$), then $\mathbf{Z} \approx \mathbf{X}$ and the baseline corrected spectra $\mathbf{X} - \mathbf{Z}$ will essentially be small-amplitude noise around the zero matrix. Hence, small values of λ are not warranted. The solution of $\mathbf{Z}(\mathbf{I} + \lambda^2 \mathbf{C}) = \mathbf{X}$ is equivalent to a sum involving the loading vectors $\mathbf{v}_{:j}$ of the derivative operator \mathbf{D} —see Eq.(12) in the Supplement. The filter factors $f_j = 1/(1 + \lambda^2 s_j^2)$ in Eq.(12) can only damp or filter the corresponding loading vector $\mathbf{v}_{:j}$ when λ is sufficiently large, i.e. ($\lambda \gg 1$). As result, we will assess performance across four penalty values: $\lambda = \{1, 10, 100, 1000\}$.

4.6 Selection of the latent dimension

As mentioned in Section 4.2, the calibration model required for predicting \mathbf{y}_2 in Step 2 in the full and partial schemes in Section 4.2 will be done using Partial Least Squares (PLS). To select the PLS latent dimension, we use an approach based on metric ranking.

Based upon the predictions on the tuning set, let's consider the MARD and R2 values across PLS latent dimensions $1, 2, \dots, 20$. The latent dimension with the lowest MARD value gets a rank of 1; the latent dimension with the second lowest MARD value gets a rank of 2; and so on. Similarly, the latent dimension with the highest R2 value gets a rank of 1; the latent dimension with the second highest R2 value gets a rank of 2; and so on. Let $[\alpha_1, \alpha_2, \dots, \alpha_{20}]$ and $[\beta_1, \beta_2, \dots, \beta_{20}]$ correspond to the integer-based rankings associated with MARD and R2, respectively, across PLS latent dimensions $1, 2, \dots, 20$. Hence, each latent dimension k is associated with a pair of ranks (α_k, β_k) , and we can treat this pair as x - and y -coordinates. The PLS latent dimension k whose coordinates (α_k, β_k) is closest to the origin $(0, 0)$ —using the Euclidean distance $\sqrt{\alpha_k^2 + \beta_k^2}$ —is deemed the optimal PLS latent dimension.

5 Performance

In this section, we examine performance for both the Milk and Cookie data sets. A collection of MARD and R2 values across 200 data partitions will be used to assess performance.

5.1 Milk data set performance

For the Milk data set, fat will be the analyte \mathbf{a} used (in tandem with the spectra \mathbf{X}) to construct the baseline spectra \mathbf{Z} . Prediction will first be assessed on urea. Performance will then be examined for all of the other analytes in order of their correlation strength with fat.

5.1.1 Fat (\mathbf{a}) and Urea (\mathbf{y})

We first examine performance where \mathbf{a} and \mathbf{y} correspond to fat and urea, respectively. Figure (4) displays the summary MARD and R2 boxplot performance across all six baseline correction methods in addition to NONE. The first and second columns correspond to the first and second derivative matrices, while the first and second rows are associated with MARD and R2, respectively. Aside from NONE, each method has four boxplots associated with it (all with the same color), and from left-to-right, these intra-method boxplots correspond to $\lambda = \{1, 10, 100, 1000\}$. We want to note several archetypal patterns of behavior:

1. The partial SPBC schemes exhibit poor performance across all λ values, and are always non-superior to NONE.
2. With respect to intra-method performance, the performance associated with $\lambda = 1$, on average, is always non-superior to the boxplots associated with $\lambda = \{10, 100, 1000\}$. This is especially the case with MARD but less so with R2.

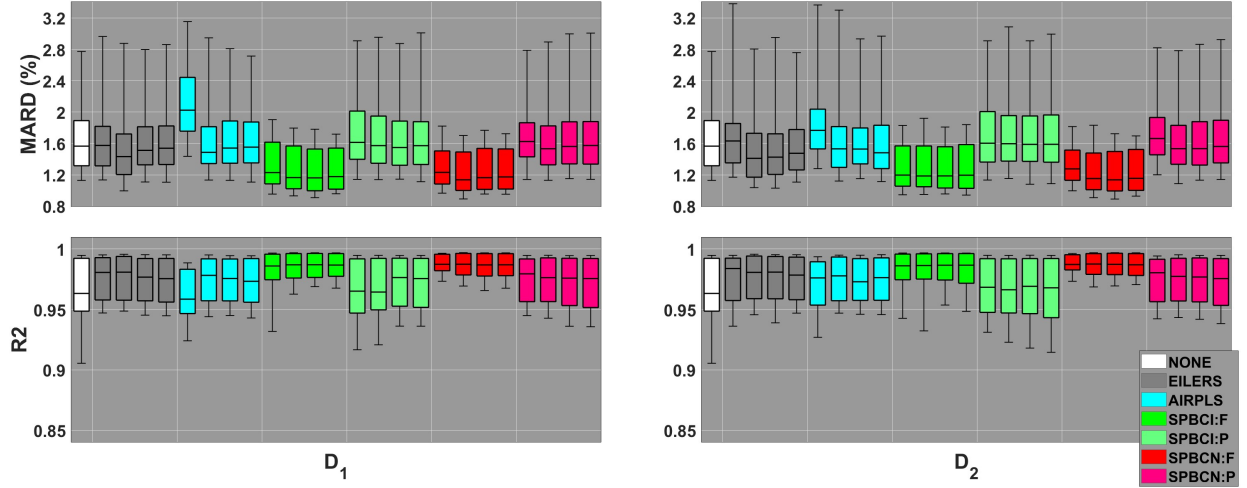


Figure 4: Urea (y) and Fat (a). Performance across baseline correction methods, and across 200 data splits. The first and second columns corresponds to the first and second derivative operators, respectively, while the first and second rows correspond to MARD and R2, respectively. Aside from NONE, each of the four boxplots associated with the same color correspond (from left-to-right) to $\lambda = \{1, 10, 100, 1000\}$.

The above performance trends hold not just for urea, but also generalize across different analytes and data sets examined in this paper. As a result, and for ease of visualization, we will heretofore focus on $\lambda = \{10, 100, 1000\}$ as well exclude the partial SPBC schemes from subsequent consideration. Figure 5 displays the resulting reduced set of boxplots, and it is clear that only SPBCI:F and SPBCN:F are superior to the other methods. Compared to NONE, the PBC approaches of EILERS and AIRPLS exhibit non-inferior performance with respect to MARD, but marginally superior R2 performance.

5.1.2 Impact of correlation between a and y

In this section, we now compare fat (a) with all the other possible analytes y (that ones that we want to predict) in order of correlation coefficient r magnitude—see Table 1. Figures 6 and 7

	Correlation Coefficient (r) of y with fat (a)				
y	lactose	protein	urea	solute	dry matter
r	0.1883	-0.4305	-0.5480	0.7771	0.9985

Table 1: Milk data set: The correlation coefficient with fat and each of the other analytes.

display MARD and R2 performance across all of these analyte pairs for instruments NIR-TM3 and NIR-TM2, respectively. For the SPBC approaches, we observe that MARD and R2 performance improves as the correlation coefficient magnitude $|r|$ increases. The improved performance with

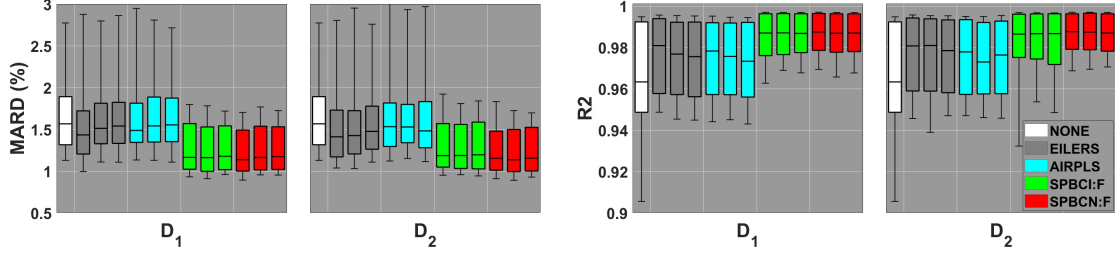


Figure 5: Fat (a) and Urea (y). Condensed performance display across `NONE`, `EILERS`, `AIRPLS`, `SPBCI:F` and `SPBCN:F` for $\lambda = \{10, 100, 1000\}$ and across 200 data splits. The first and second subplots on the left corresponds to MARD while third and fourth subplots correspond to R2. The first and third columns correspond to the first derivative operator, while the second and fourth columns correspond to the second derivative operator.

increasing $|r|$ can be explained by examining Steps 3 and 4 in Algorithms 1 and 2 (for simplicity of notation, we will drop the subscript $_{(k+1)}$ and denote $\mathbf{Z}_{(k+1)}$ as \mathbf{Z}):

$$\text{Algorithm 1: } \mathbf{Z} = \mathbf{X}(\mathbf{I} + \lambda^2 \mathbf{C})^{-1} - \mathbf{a}\mathbf{g}^T, \quad \mathbf{g} = (\mathbf{I} + \lambda^2 \mathbf{C})^{-1} \mathbf{w}$$

$$\text{Algorithm 2: } \mathbf{Z} = \mathbf{X}\mathbf{w}\mathbf{g}^T - \mathbf{a}\mathbf{g}^T, \quad \mathbf{g} = \mathbf{w}^T(\mathbf{w}\mathbf{w}^T + \lambda^2 \mathbf{C})^{-1}$$

By its very construction, the baseline spectra \mathbf{Z} is correlated with \mathbf{a} , and the baseline-corrected spectra $\mathbf{X} - \mathbf{Z}$ will likewise be correlated with \mathbf{a} . If \mathbf{a} has a strong correlation with \mathbf{y} , then the calibration model built from $\{\mathbf{X}_1 - \mathbf{Z}_1, \mathbf{y}_1\}$ should yield an improved prediction for \mathbf{y}_2 . This also explains why the partial schemes performed poorly compared to the full scheme. In the partial schemes, we obtain estimates for $\hat{\mathbf{a}}_2$ by building a calibration model from $\{\mathbf{X}_1, \mathbf{a}_1\}$ and subsequently predicting \mathbf{a}_2 from \mathbf{X}_2 . We hope that the prediction will be accurate and precise but there is no expectation that the prediction estimates will also preserve correlation. In effect, the correlation between $\hat{\mathbf{a}}_2$ and \mathbf{y}_2 has been degraded in the partial schemes.

5.2 Cookie Performance

The cookie data set allows us to explore the construction of baselines using various analytes as the correlation coefficient magnitude between \mathbf{y} and \mathbf{a} increases. Figure 8 displays performance for three pairs of analytes involving sucrose with an increasing degree of correlation coefficient magnitude. Since the response variable sucrose (\mathbf{y}) is fixed, the performance for `NONE` and the PBC methods of `EILERS` and `AIRPLS` do not change since the construction of the baselines are purely unsupervised—they do not take the analyte \mathbf{a} into account. As expected, the SPBC performance does change (as was the case with the Milk data sets) and this performance improves as the correlation coefficient magnitude $|r|$ increases. For sucrose (\mathbf{y}) and fat (\mathbf{a}), the analyte pair with the lowest correlation coefficient magnitude, none of the baseline correction methods outperform `NONE`. With respect to sucrose (\mathbf{y}) and water (\mathbf{a}), the performance is similar to what we observed with the milk

	Correlation Coefficient (r) of \mathbf{a} with sucrose \mathbf{y}		
\mathbf{a}	fat	water	flour
r	-0.1581	-0.6860	-0.9424

Table 2: Cookie data set: The correlation coefficient between sucrose and each of the other analytes.

data set, i.e., SPBCI:F and SPBCN:F exhibit superior performance compared to `NONE`, `EILERS` and `AIRPLS`. As with the milk data sets, the analytes with the strongest correlation between \mathbf{a} and \mathbf{y} yield the best performance, particularly with respect to R^2 .

6 Conclusion and Future Work

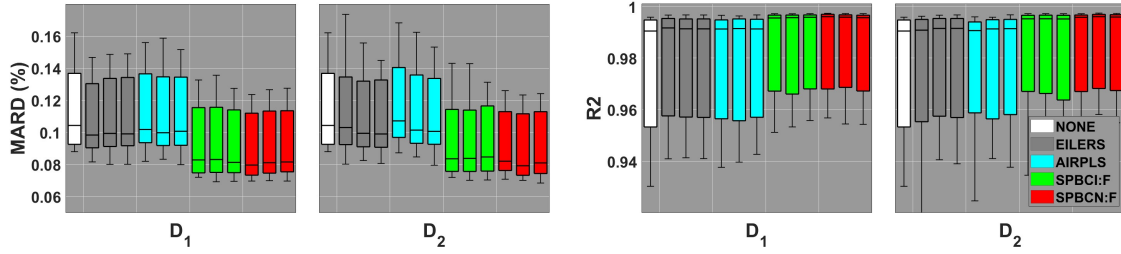
The SPBC approaches provide a simple extension for estimating baselines that incorporate a priori analyte information. There are two metaparameters (λ and latent dimension) that are relatively easy to tune, e.g., MARD and R^2 performance were observed to be qualitatively invariant across meaningful values of λ ($\lambda \gg 1$). SPBC via the full scheme provides useful baseline-corrected signals that outperform traditional state-of-the-art penalized baseline algorithms such as `AIRPLS`.

With respect to the Eilers approach in the case of $\mathbf{D} = \mathbf{D}_1$, we have developed even faster implementations (see Supplement) than Cholesky factorizations. In particular, the computation of the singular values and loading vectors of \mathbf{D}_1 using closed-form analytical formulas are novel in chemometrics. These fast implementations have been socketed into the alternating least squares framework of SPBC. Moreover, the filter factor representations discussed in the Supplement allow one to apply SPBC across multiple values of λ simultaneously.

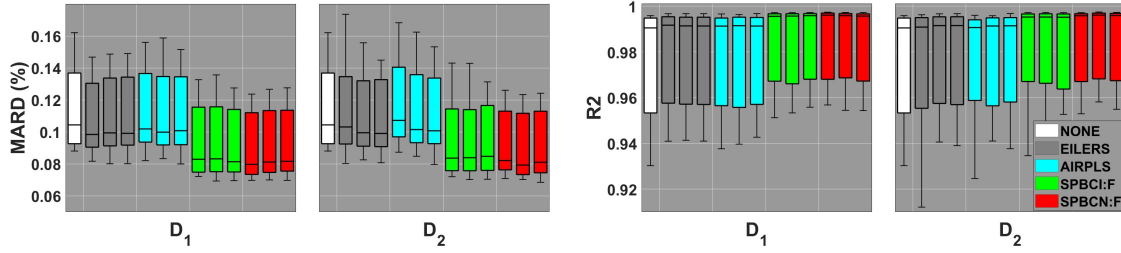
In this paper, SPBC has only been applied to NIR data sets. We would like to see if this approach can be applied to other spectroscopic modalities such as Raman spectra, fluorescence spectra, NMR signals, etc. The SPBC methods only had superior performance for the full scheme, and not for the partial scheme. We seek to develop alternative partial schemes where better estimates for $\hat{\mathbf{a}}_2$ can be obtained. Alternative schemes could include semi-supervised learning where the training data $\{\mathbf{X}_1, \mathbf{a}_1\}$ and \mathbf{X}_2 are used to compute $\hat{\mathbf{a}}_2$ (as opposed to just using the $\{\mathbf{X}_1, \mathbf{a}_1\}$). Improvements in partial scheme development will allow for more meaningful use-case scenarios and will lead to more widespread adoption. We have applied SPBC using only one analyte for \mathbf{a} . However, multiple analytes can be accommodated into a matrix $\mathbf{A} = [\mathbf{a}_1, \dots, \mathbf{a}_p]$ such that Step 3 in Algorithms 1 and 2 can be rewritten as $\mathbf{R} = \mathbf{X} - \mathbf{A}\mathbf{W}^T$ and $\mathbf{R} = \mathbf{X}\mathbf{W} - \mathbf{A}$, respectively. Moreover, one is not necessarily restricted to \mathbf{a} (or \mathbf{A}) being continuously valued reference measurements. These reference measurements could be categorical, and the regression framework employed here in this paper could be extended to classification algorithms.

Acknowledgements

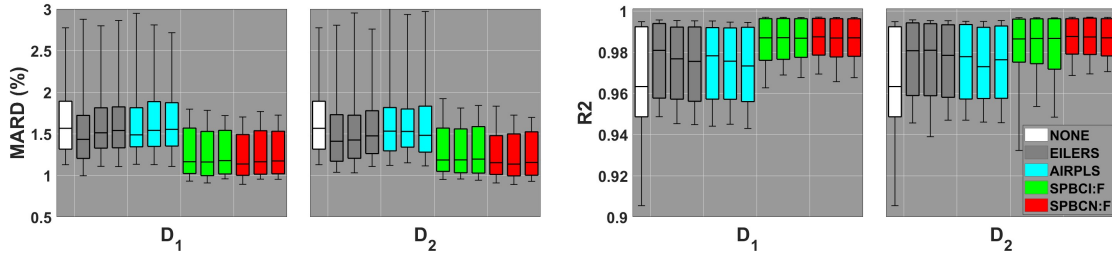
Ramin Nikzad-Langerodi acknowledges funding by the Federal Ministry for Climate Action, Environment, Energy, Mobility, Innovation and Technology (BMK), the Federal Ministry for Digital and Economic Affairs (BMDW), and the State of Upper Austria in the frame of the SCCH competence center INTEGRATE [(FFG grant no. 892418)] in the COMET - Competence Centers for Excellent Technologies Program managed by Austrian Research Promotion Agency FFG, and the FFG project zero3 (Grant No. 896399).



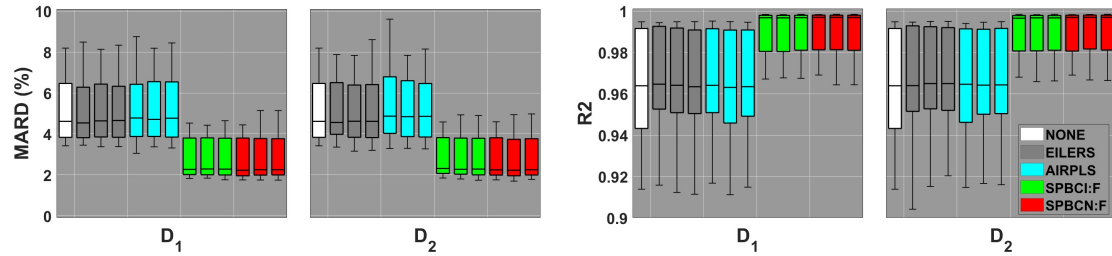
(a) Performance for fat (a) lactose (y).



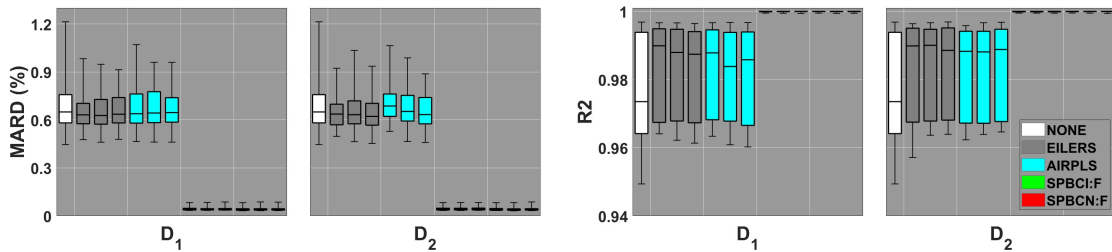
(b) Performance for fat (a) and protein (y).



(c) Performance for fat (a) and urea (y)

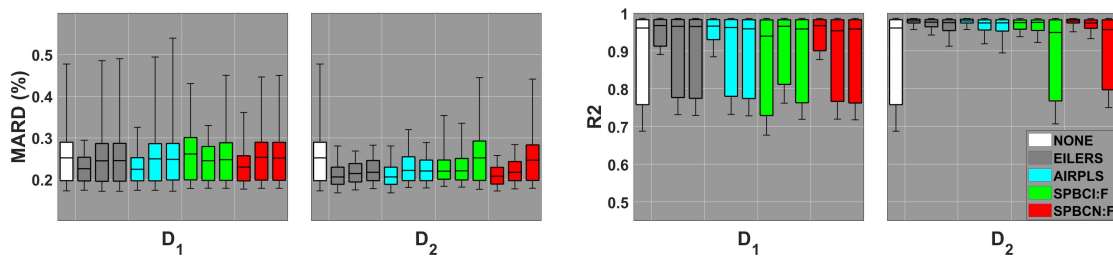


(d) Performance for fat (a) and solute (y).

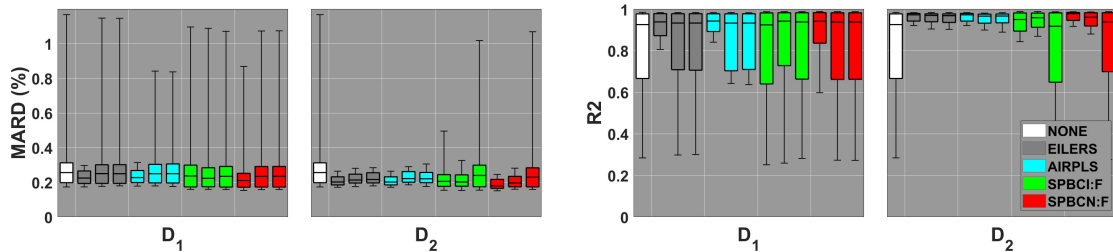


(e) Performance for fat (a) and dry matter (y).

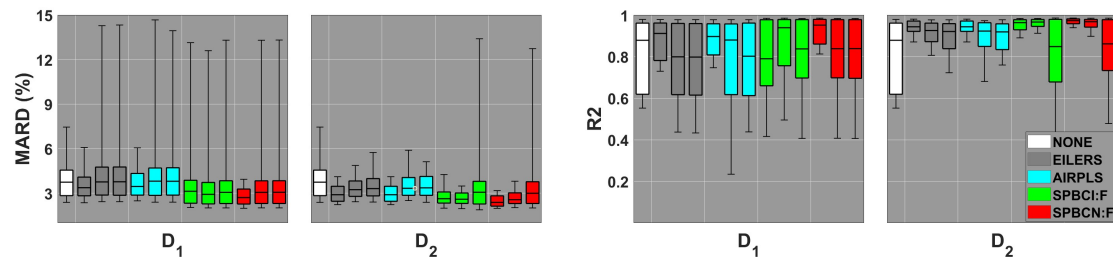
Figure 6: MARD and R2 performance for the Milk data set using instrument NIR-TM3. Description-wise, this figure has the same format as Figure 5. The correlations between fat and the other analytes are shown in 1.



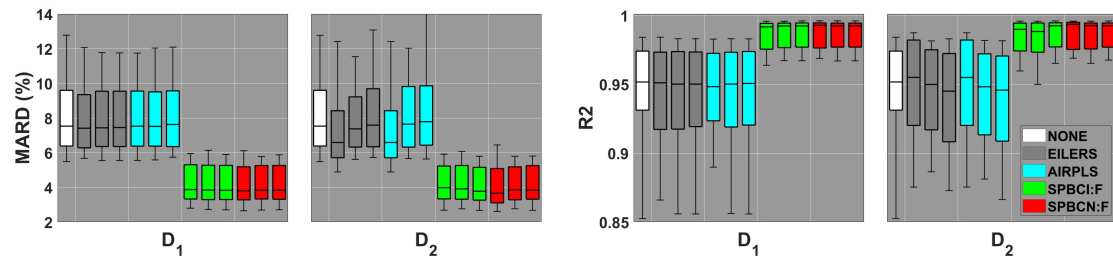
(a) Performance for fat (a) lactose (y).



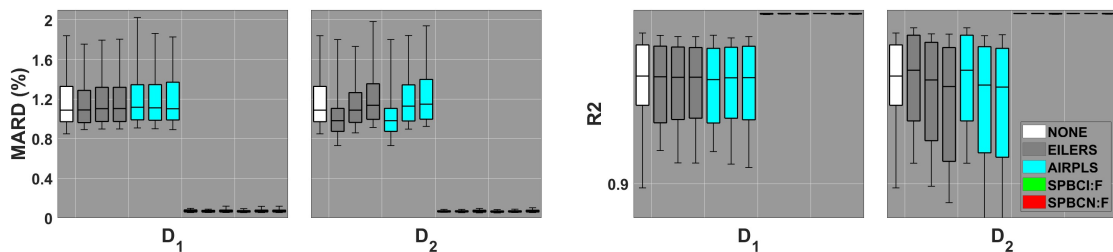
(b) Performance for fat (a) and protein (y).



(c) Performance for fat (a) and urea (y)

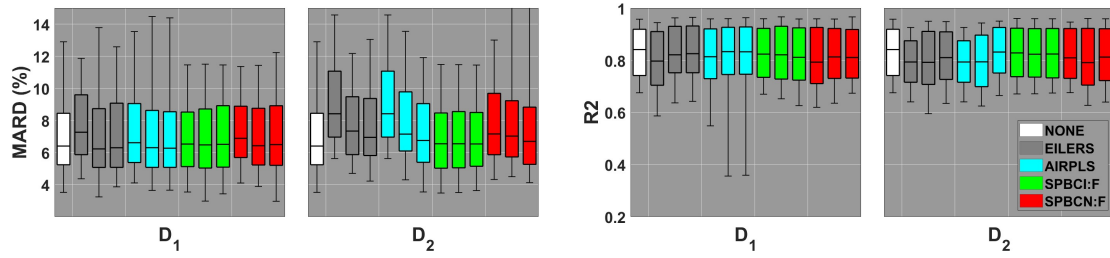


(d) Performance for fat (a) and solute (y).

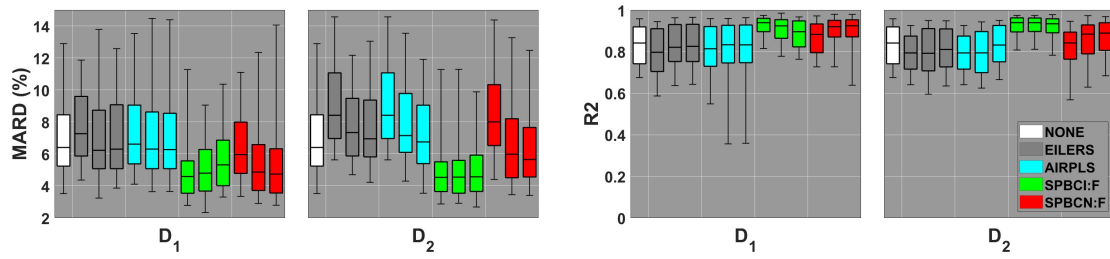


(e) Performance for fat (a) and dry matter (y).

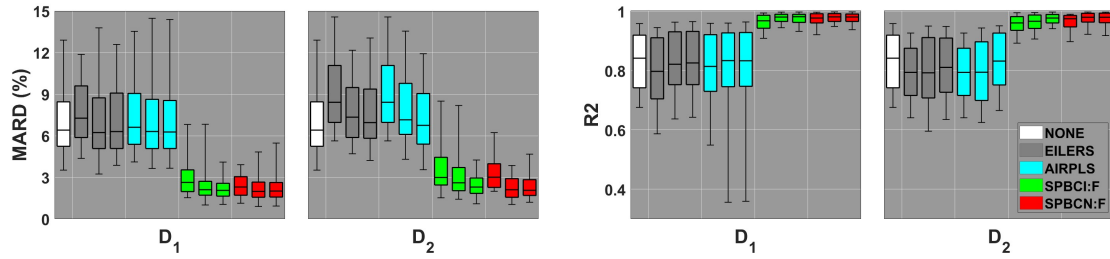
Figure 7: The display is the same as 6 except that the performance corresponds to instrument NIR-TM2.



(a) Performance for sucrose (y) and fat (a).



(b) Performance for sucrose (y) and water (a).



(c) Performance for sucrose (y) and flour (a).

Figure 8: The display is the same as Figure 6 except that the performance corresponds to the Cookie data set and its associated analytes.

Bibliography

- [1] A. Dazzi, A. Deniset-Besseau, and P. Lasch. “Minimising contributions from scattering in infrared spectra by means of an integrating sphere”. In: *Analyst* 138 (2013), pp. 4191–4201. DOI: 10.1039/c3an00381g.
- [2] A.F. Ruckstuhl et al. “Baseline subtraction using robust local regression estimation”. In: *Journal of Quantitative Spectroscopy & Radiative Transfer* 68 (2001), pp. 179–193. DOI: 10.1016/S0022-4073(00)00021-2.
- [3] I. Schecter. “Correction for Nonlinear Fluctuating Background in Monovariate Analytical Systems”. In: *Analytical Chemistry* 67 (1995), pp. 2580–2585. DOI: 10.1021/ac00111a014.
- [4] Vincent Mazet et al. “Background removal from spectra by designing and minimising a non-quadratic cost function”. In: *Chemometrics and Intelligent Laboratory Systems* 76 (2005), pp. 121–133. DOI: 10.1016/J.CHEMOLAB.2004.10.003.
- [5] Vincent Mazet et al. “Background removal from spectra by designing and minimising a non-quadratic cost function”. In: *Chemometrics and Intelligent Laboratory Systems* 76 (2005), pp. 121–133. DOI: 10.1016/J.CHEMOLAB.2004.10.003.
- [6] P. Geladi, D. MacDougall, and H. Martens. “Linearization and scatter-correction for near-infrared reflectance spectra of meat”. In: *Applied Spectroscopy* 39 (3 1985), pp. 491–500.
- [7] H. Martens and E. Stark. “Extended multiplicative signal correction and spectral interference subtraction: new preprocessing methods for near infrared spectroscopy”. In: *J Pharm Biomed Anal.* 9 (8 1991), pp. 625–635.
- [8] M. Mancini, Giuseppe Toscano, and Åsmund Rinnan. “Study of the scattering effects on NIR data for the prediction of ash content using EMSC correction factors”. In: *J Pharm Biomed Anal.* 9 (8 1991), pp. 625–635.
- [9] A. Savitzky and M.J.E. Golay. “Smoothing and differentiation of data by simplified least squares procedures”. In: *Analytical Chemistry* 36 (8 1964), pp. 1627–1639. DOI: 10.1021/ac60214a047.
- [10] M. Schmid, D. Rath, and U. Diebold. “Why and How Savitzky-Golay Filters Should Be Replaced”. In: *ACS Measurement Science* 2 (2022), pp. 185–196. DOI: 10.1021/acsmeasuresciau.1c00054.
- [11] P.H.C. Eilers. “A perfect smoother”. In: *Anal Chem* 75 (14 2003), 3631–3636. DOI: 10.1021/ac034173t.

- [12] P.H.C. Eilers and H.F.M. Boelens. “Baseline Correction with Asymmetric Least Squares Smoothing”. In: *Report (Leiden University Medical Centre)* (2005).
- [13] Z.M. Zhang, S. Chen, and Y.Z. Liang. “Baseline correction using adaptive iteratively reweighted penalized least squares”. In: *Analyst* 135 (5 2010), pp. 1138–1146. DOI: 10.1039/b922045c.
- [14] S-J. Baek et al. “Baseline correction using asymmetrically reweighted penalized least squares smoothing”. In: *Analyst* 140 (2015), pp. 250–257. DOI: 10.1039/c4an01061b.
- [15] P.C. Hansen. *Rank-Deficient and Discrete Ill-Posed Problems*. Society for Industrial and Applied Mathematics, 1998. DOI: 10.1137/1.9780898719697. URL: <https://epubs.siam.org/doi/abs/10.1137/1.9780898719697>.
- [16] K.B. Petersen and M.S. Pedersen. “The Matrix Cookbook”. In: (2012). URL: <http://www2.imm.dtu.dk/pubdb/pubs/3274-full.html>.
- [17] B.G. Osborne et al. “Application of Near-Infrared Reflectance Spectroscopy to Compositional Analysis of Biscuits and Biscuit Dough”. In: *Journal of the Science of Food and Agriculture* 35 (1 1984), pp. 99–105. DOI: 10.1002/jsfa.2740350116.
- [18] S. Uusitalo et al. “Evaluation of MEMS NIR Spectrometers for On-Farm Analysis of Raw Milk Composition”. In: *Foods* 10 (2021). DOI: 10.3390/foods10112686.
- [19] W-C Yueh. “Eigenvalues of several tridiagonal matrices”. In: *Applied Mathematics E-Notes* 5 (2005), pp. 66–74. URL: <https://www.math.nthu.edu.tw/~amen/2005/040903-7.pdf>.

Supplement: Numerical Considerations

There are many instances when the most straightforward solution of a linear system may not be the most efficient. For example, the numerical solution to the linear system $\mathbf{Z}(\mathbf{I} + \lambda^2 \mathbf{C}) = \mathbf{X}$ suggested by [11] uses Cholesky factorization on the coefficient matrix $\mathbf{I} + \lambda^2 \mathbf{C}$ via sparse matrix libraries since $\mathbf{C} = \mathbf{D}^T \mathbf{D}$ is a tridiagonal or pentadiagonal matrix if $\mathbf{D} = \mathbf{D}_1$ or $\mathbf{D} = \mathbf{D}_2$, respectively. While computationally sound, there are other implementations that are more efficient. Given that these system of linear equations are embedded in an alternative least squares loop in Algorithms 1 and 2, details involving computational speedup are warranted.

A Filter factor representation in the Eilers approach

Suppose the *reduced* Singular Value Decomposition (SVD) of $\mathbf{D} \in \mathbb{R}^{(n-k) \times n}$ yields $\mathbf{D} = \mathbf{U} \mathbf{S} \mathbf{V}^T$ where \mathbf{U} and \mathbf{V} are orthonormal and $\mathbf{S} = \text{diag}(s_1, s_2, \dots, s_{n-k})$, $k = \{1, 2\}$. The *full* SVD of \mathbf{D} similarly yields

$$\mathbf{D} = [\mathbf{U}, \mathbf{U}_\emptyset] \begin{bmatrix} \mathbf{S} & \mathbf{0} \\ \mathbf{0} & \mathbf{0} \end{bmatrix} [\mathbf{V}, \mathbf{V}_\emptyset]^T$$

where \mathbf{U}_\emptyset and \mathbf{V}_\emptyset are the orthonormal nullspace vectors of $\mathbf{D} \mathbf{D}^T$ and $\mathbf{D}^T \mathbf{D}$, respectively. We will only be interested in \mathbf{V}_\emptyset since $\mathbf{C} = \mathbf{D}^T \mathbf{D}$ in Eq.(3). Fortunately, the nullspace \mathcal{N} of \mathbf{D} is well characterized [15]: $\mathcal{N}(\mathbf{D}_1) = \text{span}(\mathbf{n}_1)$ and $\mathcal{N}(\mathbf{D}_2) = \text{span}([\mathbf{n}_1, \mathbf{n}_2])$ where $\mathbf{n}_1 = \mathbf{1}_n = [1, 1, \dots, 1]^T$ and $\mathbf{n}_2 = [1, 2, \dots, n]^T$. Using classical Gram-Schmidt orthogonalization, we obtain the orthonormal columns of \mathbf{V}_\emptyset :

$$\mathbf{v}_{\emptyset,1} = \frac{1}{\sqrt{n}} \mathbf{n}_1, \quad \mathbf{v}_{\emptyset,2} = \frac{\mathbf{n}_2 - \mu_{\mathbf{n}_2} \mathbf{n}_1}{\|\mathbf{n}_2 - \mu_{\mathbf{n}_2} \mathbf{n}_1\|_2}, \quad \mu_{\mathbf{n}_2} = \frac{1}{n} (\mathbf{1}_n^T \mathbf{n}_2) \quad (11)$$

such that $\mathbf{V}_\emptyset = \mathbf{v}_{\emptyset,1}$ and $\mathbf{V}_\emptyset = [\mathbf{v}_{\emptyset,1}, \mathbf{v}_{\emptyset,2}]$ for \mathbf{D}_1 and \mathbf{D}_2 , respectively. As a result, we can express the Eilers solution in Eq.(3) as

$$\begin{aligned} \mathbf{z} = (\mathbf{I} + \lambda^2 \mathbf{C})^{-1} \mathbf{x} &= (\mathbf{V} \mathbf{V}^T + \mathbf{V}_\emptyset \mathbf{V}_\emptyset^T + \lambda^2 \mathbf{V} \mathbf{S}^2 \mathbf{V}^T)^{-1} \mathbf{x} \\ &= \mathbf{V} \mathbf{F} \mathbf{V}^T \mathbf{x} + \mathbf{V}_\emptyset \mathbf{V}_\emptyset^T \mathbf{x}, \quad \mathbf{F} = \text{diag}(f_1, \dots, f_{n-k}), \quad f_i = \frac{1}{1 + \lambda^2 s_i^2} \end{aligned} \quad (12)$$

When $\mathbf{D} = \mathbf{D}_1$, then $\mathbf{V}_\emptyset \mathbf{V}_\emptyset^T \mathbf{x} = \frac{1}{n} \mathbf{1}_n \mathbf{1}_n^T \mathbf{x} = \mathbf{1}_n \mu_x$ where $\mu_x = (\mathbf{1}_n^T \mathbf{x})/n$ is the average value across the entries of \mathbf{x} . As a result, the baseline spectrum \mathbf{z} can be expressed as a linear combination of the loading vectors of \mathbf{D}_1 :

$$\mathbf{z} = \sum_{j=1}^{n-1} c_j \mathbf{v}_{:j} + \mu_x \mathbf{1}_n, \quad c_j = \frac{\mathbf{v}_{:j}^T \mathbf{x}}{1 + \lambda^2 s_j^2}. \quad (13)$$

The second term $(\mathbf{V}_\emptyset \mathbf{V}_\emptyset^T) \mathbf{x}$ in Eq.(12) is the fixed or *unregularized component* of the solution \mathbf{z} since the component does not depend on λ . The diagonal matrix \mathbf{F} is analogous to the filter factor matrix associated with standard Tikhonov regularization or ridge regression [15]. The contribution

of the singular vector $\mathbf{v}_{:j}$ is damped or “filtered” by its corresponding filter factor f_j . As $\lambda \rightarrow 0$, $\mathbf{F} \rightarrow \mathbf{I}$, and the solution \mathbf{z} approaches \mathbf{x} . At the other extreme, as $\lambda \rightarrow \infty$, the first term $\mathbf{V}\mathbf{F}\mathbf{V}^T\mathbf{x}$ in Eq.(12) shrinks toward zero and \mathbf{z} approaches the unregularized component $(\mathbf{V}_\emptyset\mathbf{V}_\emptyset^T)\mathbf{x}$. The SVD-based solution in Eq.(12) also has the appealing aspect in that the solution can be vectorized across multiple values of λ . Next we will discuss how the loading vectors $\mathbf{v}_{:j}$ and singular values s_i of \mathbf{D}_1 can be computed without the need of the SVD.

B The eigenstructure of $\mathbf{D} = \mathbf{D}_1$

One can exploit the tridiagonal structure of $\mathbf{C} = \mathbf{D}_1^T\mathbf{D}_1 = \mathbf{V}\mathbf{S}^2\mathbf{V}^T$ to compute the singular values and loading vectors *without the need of the SVD*. We first note that matrix \mathbf{C} is of a tridiagonal form

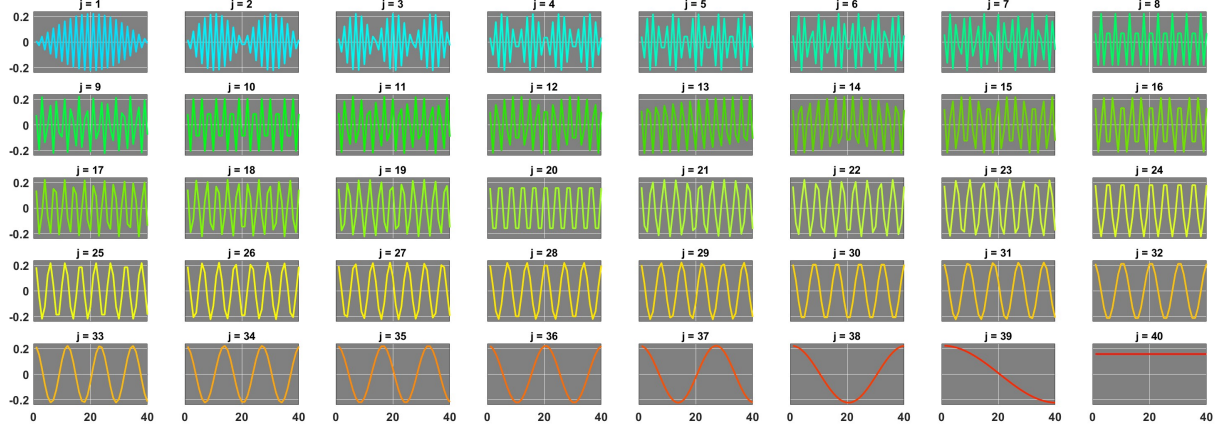
$$\mathbf{D}_1 = \begin{bmatrix} b-d & c & 0 & 0 & \cdots & 0 & 0 & 0 \\ a & b & c & 0 & \cdots & 0 & 0 & 0 \\ 0 & a & b & c & \cdots & 0 & 0 & 0 \\ \cdots & \cdots & \cdots & \cdots & \cdots & \cdots & \cdots & \cdots \\ 0 & 0 & 0 & 0 & \cdots & a & b & c \\ 0 & 0 & 0 & 0 & \cdots & 0 & a & b-d \end{bmatrix} \in \mathbb{R}^{n \times n} \quad (14)$$

where $a = c = -1$, $b = 2$ and $d = 1$. The near Toeplitz-like structure (Toeplitz matrices are banded matrices with constant diagonal elements) of Eq.(14) allows the singular values s_j and loading vectors $\mathbf{v}_{:j} = [v_{1j}, \dots, v_{nj}]^T$ of \mathbf{D}_1 to be analytically constructed using symbolic calculus[19]:

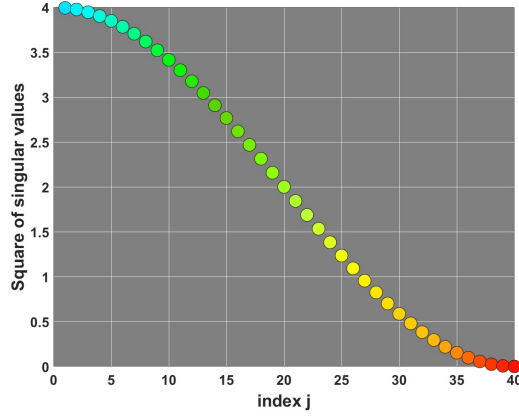
$$s_j^2 = 2 - 2 \cos \left(\frac{(n-j)\pi}{n} \right), \quad v_{ij} = \cos \left(\frac{(n-j)(2i-1)\pi}{2n} \right), \quad i, j = 1, 2, \dots, n.$$

This exploitation of the near-Toeplitz structure of $\mathbf{C} = \mathbf{D}_1^T\mathbf{D}_1$ is novel in baseline correction.

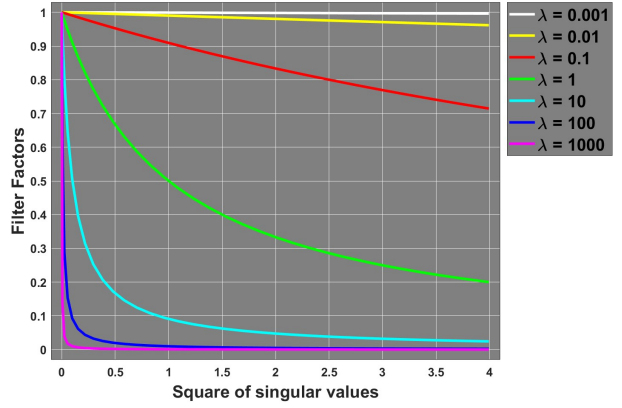
To illustrate the eigenstructure of the derivative operator, we compute the analytical-based SVD of $\mathbf{C} = \mathbf{D}_1^T\mathbf{D}_1 = \mathbf{V}\mathbf{S}^2\mathbf{V}^T$ where $n = 40$ such that $\mathbf{D}_1 = \mathbf{U}\mathbf{S}\mathbf{V}^T \in \mathbb{R}^{39 \times 40}$. Figure 9a shows the loading vectors $\mathbf{v}_{:j}$ in $\mathbf{V} = [\mathbf{v}_{:1}, \mathbf{v}_{:2}, \dots, \mathbf{v}_{:40}]$ while Figure 9b displays the square of the singular values $\{s_1^2, s_2^2, \dots, s_{40}^2\}$. The last loading vector \mathbf{v}_{40} actually corresponds to the nullspace vector $\mathbf{v}_{\emptyset,1} = \frac{1}{\sqrt{n}}\mathbf{1}_n$. Filter 9c displays the value of the filter factors $f_j = 1/(1 + \lambda^2 s_j^2)$ for $\lambda = \{0.001, 0.01, 0.1, 1, 0.10, 100, 1000\}$ —each colored curve corresponds to a different value of λ . The loading vector $\mathbf{v}_{:j}$ and singular value s_j^2 associated with each index value of j has its own color: as j increases in value, the colors vary from blue (high frequency) to red (low frequency). Compared to most matrices, the loading vectors of \mathbf{D}_1 (and \mathbf{D}_2 as well) are unusual in that the number of sign changes (the number of times v_{ij} crosses the x -axis) *decreases* as j increases. The filter factor curves indicate that the terms in Eq.(13) associated with high frequency loading vectors (the blues and greens) are easily damped by moderately large values of λ , whereas the low frequency loading vectors are preserved except for the largest values of λ .



(a) The loading vectors $\mathbf{v}_{:j} = [v_{1j}, v_{2j}, \dots, v_{40j}]^T$ associated with $\mathbf{D}_1 \in \mathbb{R}^{39 \times 40}$ are displayed. For each subplot, the y -axis corresponds to the value of v_{ij} while the x -axis corresponds to $i = \{1, 2, \dots, 40\}$.



(b) The singular values s_j^2 plotted as a function of index j .



(c) The filter factors $f_j = \frac{1}{1 + \lambda^2 s_j^2}$ plotted as a function of s_j^2 .

Figure 9: The loadings vectors, singular and filter factors are displayed for a first derivative operator matrix $\mathbf{D}_1 \in \mathbb{R}^{39 \times 40}$.

C Filter Factor Representations in SPBCN and SPBCI

For SPBCN, Step 4 of Algorithm 1, i.e., $\mathbf{Z}_{(k+1)} = \mathbf{R}(\mathbf{I} + \lambda^2 \mathbf{C})$ (where $\mathbf{R} = \mathbf{X} - \mathbf{a}\mathbf{w}^T$) is the computational bottleneck of the alternating least squares procedure. Its solution is the same as Eq.(12) except that the matrix \mathbf{X} is replaced with \mathbf{R} :

$$\mathbf{Z}_{(k+1)} = \mathbf{R} (\mathbf{V}\mathbf{F}\mathbf{V}^T + \mathbf{V}_\emptyset \mathbf{V}_\emptyset^T) \mathbf{R}\mathbf{V}\mathbf{F}\mathbf{V}^T + \mathbf{R}\mathbf{V}_\emptyset \mathbf{V}_\emptyset^T, \quad (15)$$

For SPBCI, let $\mathbf{X} = \mathbf{P}\mathbf{\Sigma}\mathbf{Q}^T$ be the *reduced* Singular Value Decomposition (SVD) of \mathbf{X} where \mathbf{P} and \mathbf{Q} are orthonormal and $\mathbf{\Sigma} = \text{diag}(\sigma_1, \sigma_2, \dots, \sigma_r)$ where r is the rank \mathbf{X} . Similarly, let

$$\mathbf{X} = [\mathbf{P} \quad \mathbf{P}_0] \begin{bmatrix} \mathbf{\Sigma} & \mathbf{0} \\ \mathbf{0} & \mathbf{0} \end{bmatrix} [\mathbf{Q} \quad \mathbf{Q}_0]^T$$

be the *full* SVD where $\text{span}(\mathbf{Q}_0)$ is the nullspace of \mathbf{X} . In Step 2 of Algorithm 2, the linear system $\mathbf{B}^T \mathbf{B} \mathbf{w} = \mathbf{B}^T \mathbf{a}$ where $\mathbf{B} = \mathbf{X} - \mathbf{Z}_{(k)}$ can then be rewritten as

$$\mathbf{X}^T \mathbf{X} \mathbf{w} = \mathbf{d}_{(k)}, \quad \mathbf{d}_{(k)} = \mathbf{X}^T \mathbf{a} + \mathbf{B}^T \mathbf{Z}_{(k)} \mathbf{w} + \mathbf{Z}_{(k)}^T (\mathbf{X} \mathbf{w} - \mathbf{a}) \quad (16)$$

In this case, the coefficient matrix $\mathbf{X}^T \mathbf{X}$ on the left-hand-side is constant, and as a result, the solution can be expressed using the basis vectors in \mathbf{Q} and \mathbf{Q}_0 . Due to the high correlation of spectra in \mathbf{X} , instead of solving $\mathbf{X}^T \mathbf{X} \mathbf{w} = \mathbf{d}_{(k)}$ in Step 2 of Algorithm 2, we will instead solve $(\mathbf{X}^T \mathbf{X} + \tau^2 \mathbf{I}) \mathbf{w} = \mathbf{d}_{(k)}$ via ridge regression.² As result, the solution \mathbf{w} in Step 2 can be written as

$$\mathbf{w} = \mathbf{Q} \mathbf{F} \mathbf{Q}^T \mathbf{d}_{(k)} + \mathbf{Q}_0 \mathbf{Q}_0^T \mathbf{d}_{(k)} \quad \text{where} \quad \mathbf{F} = \text{diag}(f_1, \dots, f_r), \quad f_i = \frac{1}{\sigma_i^2 + \tau^2}$$

If \mathbf{X} has full column rank, i.e., $m \geq n$ and $r = n$, then \mathbf{Q}_0 will empty and the solution can be written as $\mathbf{w} = \mathbf{Q} \mathbf{F} \mathbf{Q}^T \mathbf{d}_{(k)}$. Since the ridge regression occurs within an alternative least squares loop, it is prudent to compute the SVD of \mathbf{X} once at the very beginning of the loop, and then re-use the pre-computed SVD components (the singular values in Σ , and the loading vectors in \mathbf{Q} and the nullspace vectors in \mathbf{Q}_0) over-and-over again.

²The ridge parameter will be intentionally chosen to be small to ensure numerical stability. We will not try to optimize $\tau > 0$ as a tuning parameter.